Journal of Alloys and Compounds 480 (2009) 193–197

Contents lists available at ScienceDirect

Journal of Alloys and Compounds

journal homepage: www.elsevier.com/locate/jallcom

Influence of cooling field on the magnetic properties of Ni/NiO nanostructure

M. Thakur, M. Patra, S. Majumdar, S. Giri*

Department of Solid State Physics and Center for Advanced Materials, Indian Association for the Cultivation of Science, Jadavpur, Kolkata 700 032, India

ARTICLE INFO

Article history:
Received 15 December 2008
Received in revised form 30 January 2009
Accepted 31 January 2009
Available online 10 February 2009

PACS:
75.50.Tt
75.50.Lk
77.80.Dj

Keywords:
Nanocrystalline materials
Magnetic hysteresis
Exchange bias

ABSTRACT

Nanoparticles of Ni/NiO structure were prepared by sol–gel route followed by the annealing in presence of controlled oxygen and argon gas mixture. When the sample was cooled down to 5 K from room temperature in a static magnetic field, a systematic shift of the magnetic hysteresis loop was observed. The shift was absent when the sample was cooled in zero field. For cooling the sample in field-cooled mode a small horizontal shift was noticed along with a moderate vertical shift of the hysteresis loop at the saturation of magnetization, which indicates the typical manifestation of exchange bias effect. The horizontal shift increases with decreasing particle size retaining almost unchanged relative vertical shift, where vertical shift is found to be uncorrelated with the horizontal shift. The exchange bias like effect in the Ni/NiO nanostructure is suggested at the Ni/NiO interface, where Ni is ferromagnetic and NiO is in the disordered magnetic state.

1. Introduction

Exchange bias (EB) effect is a manifestation of induced unidirectional anisotropy in a heterogeneous system composed of ferromagnetic (FM) and antiferromagnetic (AFM) substances when the system is cooled through the Néel temperature in a static magnetic field [1–6]. First observation of EB phenomenon was reported by Meiklejohn and Bean in Co/CoO core–shell structure at the FM/AFM interface [1]. Observation of EB in nanoparticles has been reported for a wide variety of materials and morphologies, where some of the largest observed EB effects have been reported for the particles consisting of a FM core and an antiferromagnetic or ferrimagnetic (FI) or spin-glass (SG) shell structure [6].

The EB effect is experimentally observed by the systematic horizontal and vertical shifts of the magnetic hysteresis (MH) loops. The horizontal shift of the MH loop is defined as EB field (H_E), whereas the vertical shift at the saturation of magnetization is defined as EB magnetization (M_E). Recently, large horizontal shift of the MH loop exhibiting EB effect has been reported for Ni/NiO nanostructure when the sample was cooled in field-cooled (FC) mode [7–10]. Unlike the reported results we observe a very small horizontal shift associated with a moderate vertical shift at 5 K in Ni/NiO nanostructures, where both the shifts are uncorrelated with each other for different nanostructures. The EB like feature is suggested here at the Ni/NiO interface, where Ni is ferromagnetic and NiO is in the disordered magnetic state.

2. Experiment

Nanoparticles of Ni/NiO structure were prepared by the sol–gel route [11]. The aqueous solution of nickel(II) nitrate was prepared by dissolving Ni (Aldrich 99.99%) powder in the nitric acid. A proper amount of citric acid (Loba Chemie 99.5%) was added to the solution of the nickel(II) nitrate and stirred for 4 h to achieve the homogeneous nickel citrate solution, where the temperature of the solution was kept around 60 °C. The amount of citric acid was chosen to ensure all the metal ions to form metal citrate by considering that only two of the citrate ions take part in chemical bonding with a metal ion [11]. The clear solution was poured into a beaker and allowed to form gel gently in air, which was kept at 70 °C. Thermogram of thermogravimetric analyzer (TA instrument, SDT Q600) indicates that the decomposition of dried gel was almost completed around ~ 325 ° C by evolving a number of gases viz., CO, CO_2, NO_2, O_2 water vapour, etc. Here the dried gel was decomposed at 350 and 450 ° C for 5 h in a flow of mixture gas consisting of oxygen and argon. For simplicity we address the samples as S1 and S2, which were heated at 450 and 350 °C, respectively.

Transmission electron microscopy (TEM) was carried out by using a JEOL TEM, 2010 microscope. The crystalline phase was identified by powder X-ray diffraction patterns (XRD) of the samples by using a BRUKER axs (Model: 8D - ADVANCE) diffractometer with a Cu Kα radiation source. The magnetization (M) was measured using a commercial superconducting quantum interference device (SQUID) magnetometer (MPMS, XL).

3. Experimental results and discussions

TEM image of the sample S1 is shown in Fig. 1, which indicates that particles are well separated from each other in most of the cases despite any protective layer or surfactant was not used

* Corresponding author. Tel.: +91 33 2473 4971; fax: +91 33 2473 2805.
E-mail address: sspsg2@iacs.res.in (S. Giri).

0925-8388/$ – see front matter © 2009 Elsevier B.V. All rights reserved.
doi:10.1016/j.jallcom.2009.01.128

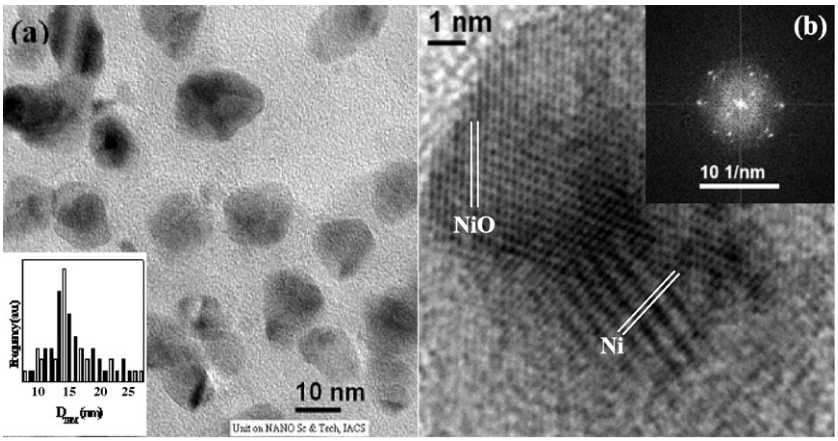

Fig. 1. (a) TEM image of S1. Inset exhibits the histogram of particle size distributions. (b) HRTEM image indicating different planes corresponding to Ni and NiO. Inset exhibits the FFT of the HRTEM image.

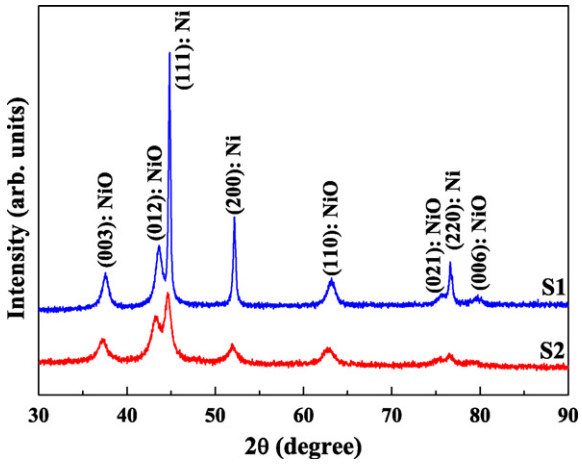

Fig. 2. X-ray powder diffraction patterns of S1 and S2, where the planes corresponding to Ni and NiO are indicated in the figure.

during synthesis. Since the final heating was performed at 550 ° C for 5 h, the residual amorphous carbon may be left during decomposition of metal citrate which typically disappears in terms of CO and CO_2 gases while heating above 800 ° C [11]. Large distribution of particle size (D_{TEM}) from 8 to 27 nm is shown in the inset of Fig. 1(a) with average size of the particles around ∼ 14 nm. High resolution TEM (HRTEM) image is shown in Fig. 1(b), where two different overlapped lattice fringes corresponding to Ni and NiO are highlighted in the figure. The fast fourier transformation (FFT) of the HRTEM image is shown in the inset of Fig. 1(b), where FFT of the image clearly confirms the existence of two different planes corresponding to the Ni and NiO. X-ray powder diffraction patterns of S1 and S2 are shown in Fig. 2. Diffraction peaks corresponding to different planes of coexisting Ni and NiO are shown in the figure. The width of the diffraction peaks are decreased while the intensities are increased for S1 than that of S2, which indicates that the average size of S2 is decreased compared to S1. The estimate of the particle size using Scherrer's formula are shown in Table 1 for S1 and S2 [12]. The values of the particle size (D_{XRD}) obtained from Scherrer's formula are found to be much larger than the average size (∼ 14 nm) obtained from TEM, despite the values of D_{XRD} agree well with the range of D_{TEM} in between 8 and 27 nm. In fact, the difference between TEM and XRD results may be ascribed to the different averaging processes of each technique while the number averaging is typically utilized in TEM and volume averaging is used in XRD. Since the number of large particles is usually small in number averaging processes its relative weight on the average is small. On the other hand, the large particles contribute considerably even if, their number is small when the volume is taken into account. Thus, volume average procedures lead to the averaging over the larger particles. The difference between TEM and XRD becomes considerable for a broad particle size distributions.

Temperature variation of zero-field-cooled (ZFC) and field-cooled (FC) magnetization measured in the heating and cooling cycles, respectively at 100 Oe are shown in the top panel of Fig. 3. We do not observe any peak in the ZFC magnetization up to 300 K which indicates that blocking temperature (T_B) is above room temperature. We note a wide distribution of particle size from 8 to 27 nm in the TEM image, where large T_B above room temperature is reasonable for the particles around ∼ 27 nm in size, which seems to be quite high for the size around ∼ 8 nm. In case of wide distribution of particle size the distribution of blocking temperature is expected exhibiting a broadened maximum in the temperature dependence of ZFC magnetization, where larger particles contribute dominating role to the magnetization than that of the smaller particles. As a result of it, the overall behaviour might be reflected through the large value of T_B corresponding to the larger particles. However, the scenario becomes complex when the interparticle interaction is taken into account. The FC magnetization in the cooling cycle exhibits a broadened maximum (T_P) indicated by the arrow in the

Table 1
Range of particle size from TEM (D_{TEM}) and average size from X-ray diffraction (D_{XRD}), coercivity (H_c), EB field (H_E), EB magnetization (M_E), saturation of magnetization (M_S) and M_E/M_S for S1 and S2.

Sample	D_{TEM} (nm)	Phase	D_{XRD} (nm)	H_C (Oe)	H_E (Oe)	M_E (emu/g)	M_S (emu/g)	M_E/M_S ($\times 10^{-2}$)
S1	8–27	Ni	27	90	7	0.40	28.3	1.4
		NiO	9					
S2	–	Ni	8	274	27	0.24	14.1	1.7
		NiO	6					

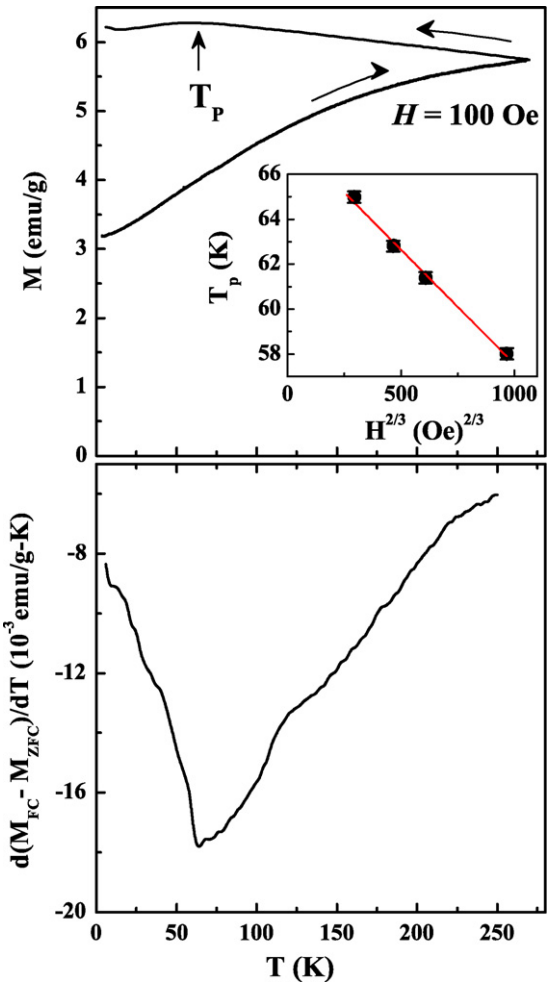

Fig. 3. (Top panel) Temperature variation of zero-field-cooled (M_{ZFC}) and field-cooled (M_{FC}) magnetization in the heating and cooling cycles, respectively, which are indicated by the arrows for S1. Position of peak (T_P) in the field-cooled magnetization is indicated by the arrow. The linear plot of T_P against $H^{2/3}$ is shown in the inset. (Bottom panel) Plot of $d(M_{FC} - M_{ZFC})/dT$ as a function of temperature.

figure. The plot of $d(M_{FC} - M_{ZFC})/dT$ as a function of temperature is shown in the bottom panel, which shows a deep in the plot around ~ 63 K, where T_P is noticed in the FC magnetization. The value of T_P shows increasing trend with increasing field and then decreases with the further increase of field in the high field region. We note systematic behaviour of T_P against $H^{2/3}$ in between 5 and 30 kOe, where the plot of T_P against $H^{2/3}$ fits satisfactorily with the Almeida–Thouless (AT) relation as $T_P \propto H^{2/3}$ shown in the inset of Fig. 3[13]. The H dependence of T_P following AT line may indicate that T_P behaves like a spin freezing temperature.

The small shift of the MH loop is observed at 5 K for S1 when the sample was cooled down to 5 K from 300 K in FC mode with cooling field, $H_{cool} = 50$ kOe. The shift is absent while cooling under ZFC condition. The MH loops measured in between ±10.0 kOe clearly exhibits the saturating tendency of magnetization at 10 kOe. A distinct vertical shift in the positive magnetization axis is observed at the saturation of magnetization shown in Fig. 4 indicated by the broken curve, where vertical shift of the magnetization close to the saturation (at 10 kOe) is defined as EB magnetization (M_E) [14]. Furthermore, a small negative shift in the field axis is also observed (not shown in Fig. 4), which is defined as EB field (H_E). The values of H_E and M_E at 5 K measured under identical condition are given in Table 1 for S1 and S2. Such a small value of H_E has also been observed in Ni/NiO bilayer film [15]. The value of coercive field (H_C) and saturation of magnetization (M_S) are also given in the table. The value of H_C is increased from 90 to 270 Oe while M_S is decreased from 28.3 to 14.1 emu/g for S1 and S2, respectively. We note that the value of H_E is larger for S2 than S1, which is reasonable with the model proposed by Meiklejohn with the relation as $H_E \approx J_{ex}/M_{FM} \times t_{FM}$ [16]. In the above expression J_{ex} is the exchange constant across the FM/AFM interface per unit area, whereas M_{FM} and t_{FM} are the magnetization and the thickness of the FM layer, respectively. In the present observation, the average size of the FM cluster analogous to t_{FM} and also M_{FM} are larger for S1 than that of S2 resulting in the considerable decrease of H_E for S1. Despite the value of H_E changes considerably, the value of M_E/M_S is remained almost unchanged for S1 and S2. Dobrynin et al. recently reported the similar behaviour of H_E and M_E for Co-core and CoO-shell structure embedded in the Al_2O_3 matrix, where a distinct vertical shift was observed without any horizontal shift in the field axis [17].

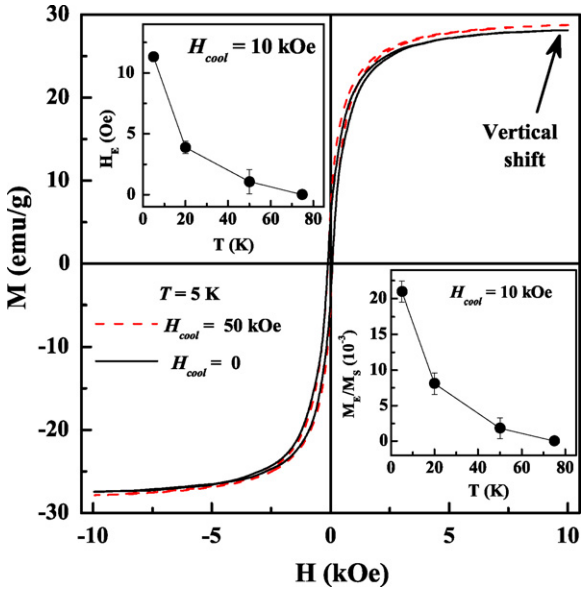

Fig. 4. Magnetic hysteresis loops at 5 K while the sample was cooled in zero field and 50 kOe for S1. Exchange bias field (H_E) and relative vertical shift (M_E/M_S) are plotted with temperature in the top and bottom inset, respectively.

In the top and bottom inset of Fig. 4 the values of H_E and M_E/M_S are plotted as a function of temperature, where the values are decreased with increasing temperature and vanish in between 50 and 75 K which is close to T_P. The cooling field (H_{cool}) dependence of EB effect was further investigated for S1. H_E and M_E/M_S as a function of H_{cool} are plotted in the top and bottom panel of Fig. 5, respectively. Initially, M_E/M_S increases and then it remains almost unaltered above 10 kOe. Despite the value of H_E is very small, it shows a systematic change with H_{cool}, where it increases initially and then decreases up to ~ 40% for the increase of H_{cool} from 10 to 50 kOe. The results are similar to the H_{cool} dependence of EB effect in Fe/iron oxides with core–shell structure [18], where EB effect is involved with FM core and SG or disordered magnetic shell. When the sample is cooled down to low temperature in the FC mode, the shift of the loop is ascribed to the pinning of the FM spins at the interface by the rigid AFM or SG spins. In case of small cooling field, H_E increases sharply with H_{cool}, which is attributed to the alignment of pinned FM spins toward the direction of H_{cool}. When all the pinned spins are aligned, the increase of H_{cool} cannot contribute to the increase of H_E above a certain limit of H_{cool}. Furthermore, large H_{cool} strongly influences the SG or disordered magnetic spins resulting in a considerable decrease of H_E, which has been observed in various systems involved with the FM/SG or disordered magnetic interface [18–20].

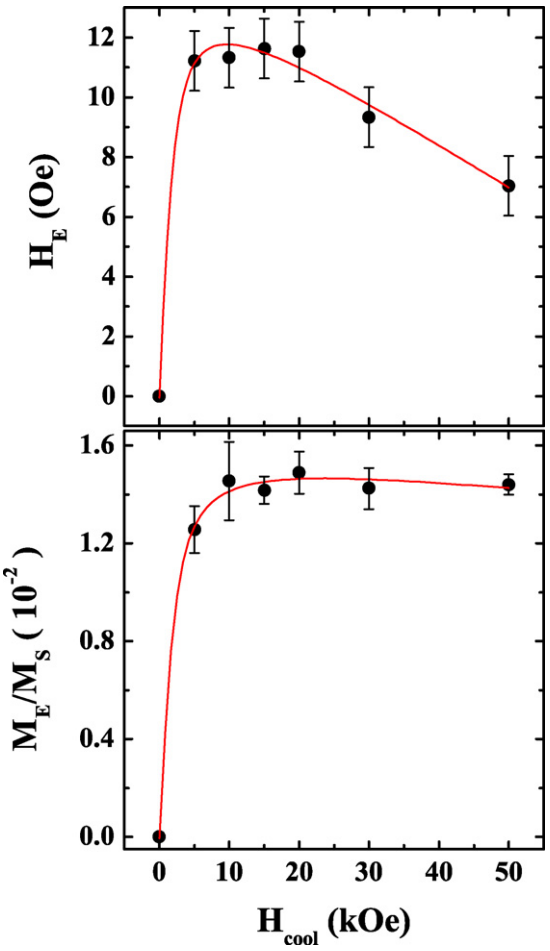

Fig. 5. Cooling field (H_{cool}) dependence of exchange bias field (H_E) (top panel) and relative vertical shift M_E/M_S (bottom panel).

The system exhibiting EB effect must have two different magnetic phases comprising of reversible spins with low magnetic anisotropy and rigid spins having strong anisotropy. Ferromagnetic spins of Ni are reversible, whereas spins in NiO have moderately stronger anisotropy than Ni spins. Bulk NiO is antiferromagnetic [21]. Nanocrystalline NiO typically exhibits the structural disorder at the surface, which may lead to the random magnetic anisotropy and frustration of competing magnetic interactions resulting disordered magnetic behaviour [9,10,22,23]. The signature of spin freezing is indicated by the broad maximum at T_P in the FC magnetization and the sharp deep at T_P in the plot of $d(M_{FC} - M_{ZFC})/dT$ with T. We further note that T_P follows the AT line supporting the spin freezing at T_P. We note that H_E and M_E/M_S vanish above T_P, where disordered magnetic spins of NiO cannot apply pinning force on the ferromagnetic spins above T_P. Previous reports [7–10] on the observation of EB effect in Ni/NiO nanostructure exhibits the large H_E in contrast to the present investigation, where the small values of H_E is observed. Bianco et al. reported large H_E in case of ball milled sample with Ni/NiO nanostructure, where Ni/NiO grains are in direct physical contact. Observation of EB effect strongly depends on the types of nanostructure, direct physical contact and the matrix among the particles, which are nicely demonstrated by Skumryev et al. [24]. EB effect was vanished while Co/CoO core–shell nanostructures are embedded in the Al_2O_3matrix. Large EB effect was observed when Co/CoO core–shell nanostructure are measured in pelletized form. Maximum EB effect was observed when the same nanostructures are embedded in the AFM (CoO) matrix. Nogués et al. recently reported that H_E significantly changes as a function of in-plane coverage density from 3.5% to 15% [25]. A strong thickness dependence of CoO layer on EB effect was reported by Tracy et al., where thin layer ($\sim$ 1 nm) of CoO shell does not show EB effect [26]. Dobrynin et al. recently reported a considerable vertical shift without any horizontal shift of the hysteresis loop for Co/CoO core–shell nanostructures embedded in the Al_2O_3matrix [17]. TEM image in the present investigation indicates that grains having Ni/NiO nanostructure do not have any direct physical contact with each other, which might be the origin of small value of H_E associated with a moderate value of M_E. In addition, the weaker anisotropy of NiO compared to CoO has a significant role on EB effect, which may lead to the observed effects [27]. If one assumes that exchange bias is a purely interface effect, then H_E as well as M_E should be normalized by the interface area. The uncorrelated results of H_E and M_E for the samples S1 and S2 might be attributed to the different Ni/NiO nanostructures, which are not exactly homogeneous core–shell structure.

4. Conclusions

In conclusion, exchange bias like effect is observed in the Ni/NiO nanostructures, where very small horizontal shift is observed associated with a moderate vertical shift. The horizontal shift increases with decreasing particle size retaining almost unchanged relative vertical shift, where vertical shift appears to be uncorrelated with the horizontal shift. The exchange bias effect in the Ni/NiO nanostructure is suggested at the Ni/NiO interface, where Ni is ferromagnetic and NiO is in the disordered magnetic state.

Acknowledgements

One of the authors (S.G.) wishes to thank DST (Project No. SR/S2/CMP-46/2003), India for the financial support. The particle size of the sample was measured by TEM under the scheme of Nanoscience and Nanotechnology initiative of DST at IACS, Kolkata, India. Authors wish to thank Mr. S. Das for recording the HRTEM image.

References

[1] W.H. Meiklejohn, C.P. Bean, Phys. Rev. 102 (1956) 1413.
[2] J. Nogues, J. Sort, V. Langlais, V. Skumryev, S. Surinach, J.S. Munoz, M.D. Baro, Phys. Rep. 422 (2005) 65.
[3] J. Nogues, J. Sort, V. Langlais, V. Skumryev, S. Surinach, J.S. Munoz, M.D. Baro, Int. J. Nanotechnol. 2 (2005) 23.
[4] J. Nogues, I.K. Schuller, J. Magn. Magn. Mater. 192 (1999) 203.
[5] R.L. Stamps, J. Phys. D: Appl. Phys. 33 (2000) R247.
[6] O. Iglesias, A. Labarta, X. Batlle, J. Nanosci. Nanotechnol. 8 (2008) 2761.
[7] M. Fraune, U. Rüdiger, G. Güntherodt, S. Cardoso, P. Freitas, Appl. Phys. Lett. 77 (2000) 3815.
[8] S. Li, M. Liu, H. Bi, L. Lü, W. Zou, Z. Huang, Y. Du, J. Alloys Compd. 425 (2006) 1.
[9] L. Del Bianco, F. Boscherini, A.L. Fiorini, M. Tamisari, F. Spizzo, E. Piscopiello, Phys. Rev. B 77 (2008) 094408.
[10] L. Del Bianco, F. Boscherini, M. Tamisari, F. Spizzo, M.V. Antisari, E. Piscopiello, J. Phys. D: Appl. Phys. 41 (2008) 134008.
[11] R.N. Panda, J.C. Shih, T.S. Chin, J. Magn. Magn. Mater. 257 (2003) 79.
[12] B.D. Cullity, Elements of X-ray Diffractions, Reading, MA, 1978.
[13] J.R.L. de Almeida, D.J. Thouless, J. Phys. A 11 (1978) 983.
[14] J. Nogués, C. Leighton, I.K. Schuller, Phys. Rev. B 61 (2000) 1315.
[15] P.Y. Yang, C. Song, F. Zeng, F. Pan, Appl. Phys. Lett. 92 (2008) 243113.
[16] W.H. Meiklejohn, J. Appl. Phys. 33 (1962) 1328.
[17] A.N. Dobrynin, D.N. Ievlev, K. Temst, P. Lievens, J. Margueritat, J. Gonzalo, C.N. Afonso, S.Q. Zhou, A. Vantomme, E. Piscopiello, G. Van Tendeloo, Appl. Phys. Lett. 87 (2005) 012501.
[18] L. Del Bianco, D. Fiorani, A.M. Testa, E. Bonetti, L. Signorini, Phys. Rev. B 70 (2004) 052401.
[19] M. Patra, K. De, S. Majumdar, S. Giri, Eur. Phys. J. B 58 (2007) 367.
[20] M. Thakur, M. Patra, K. De, S. Majumdar, S. Giri, J. Phys. Condensed Matter 20 (2008) 195215.
[21] Landolt-Börnstein, BandIII/27g, Springer, Berlin, 1993.

[22] R.H. Kodama, S.A. Makhlouf, A.E. Berkowitz, Phys. Rev. Lett. 79 (1997) 1393.
[23] E. Winkler, R.D. Zysler, M. Vasquez Mansilla, D. Fiorani, D. Rinaldi, M. Vasilakaki, K.N. Trohidou, Nanotechnology 19 (2008) 185702.
[24] V. Skumryev, S. Stoyanov, Y. Zhang, G. Hadjipanayls, D. Givord, J. Nogués, Nature 423 (2003) 850.
[25] J. Nogués, V. Skumryev, J. Sort, S. Stoyanov, D. Givord, Phys. Rev. Lett. 97 (2006) 157203.
[26] J.B. Tracy, D.N. Weiss, D.P. Dinega, M.G. Bawendi, Phys. Rev. B 72 (2005) 064404.
[27] M.S. Lund, W.A.A. Macedo, K. Liu, J. Nogués, I.K. Schuller, C. Leighton, Phys. Rev. B 66 (2002) 054422.